DYNAMICS OF FLUCTUATIONS AT THE ICE-WATER INTERFACE DURING SOLIDIFICATION

Abhandlung
zur Erlangung
des Titels eines Doktors der Naturwissenschaften
der
EIDGENOESSISCHEN TECHNISCHEN
HOCHSCHULE ZUERICH

vorgelegt von

H A N N E S G U E T T I N G E R
Dipl. Phys. ETH
geboren am 4. Dezember 1946
von Horgen (Kanton Zürich)

Angenommen auf Antrag von

Prof.Dr. W. Känzig, Referent

Prof.Dr. H. Gränicher, Korreferent

1978

Meiner Mutter

Leer - Vide - Empty

Contents

ABSTRACT

The 488 nm radiation of an argon laser is scattered quasi-elastically at the [0001] -face (basal plane) of a growing ice crystal. The scattering plane is the basal plane. The Rayleigh-linewidth is proportional to the square of the scattering vector. One measures about 2 krad/s at a scattering angle of 90^{o}. The linewidth does not depend on the growth rate. Scattering is only observed once a critical growth rate v_{crit} = 1,5 µm/s has been exceeded. Then the scattering intensity depends linearly on the growth rate in the range between 0,03 µm/s and 2,5 µm/s. Once the surface is molten scattering vanishes and does not reappear until the growth rate has again exceeded the threshold v_{crit}. The coherence properties of the scattered light indicate that the thickness of the scattering layer is less than 6 µm. The observations are interpreted in terms of a fluctuating interface. The decay time of the fluctuations has been calculated. Satisfactory agreement with the observed Rayleigh linewidth is obtained.

1. INTRODUCTION

The solid-liquid transition is one of the least understood phase transitions in particular with regard to its dynamics. The interest in crystal growth has stimulated experimental and theoretical studies of the stability of the interface at nonequilibrium conditions [1-3]. Solidification and melting are not inverse processes although the understanding of one process may supplement the understanding of the other [4].

There are many thorough investigations of the changes that occur in the bulk solid if the melting temperature is approached [5,6]. A difficulty in these experiments arises because the impurities are not homogeneously distributed and affect the melting temperature.

Several theories extrapolate solid state properties to an instability point where long range order vanishes. Lindemann's melting criterion based on the vibrational instability of the lattice successfully relates the melting temperature to mechanical properties [7]. This model was further elaborated by Born and Brillouin [8,9] who studied the elastic shear modulus. In a recent paper [10] a great variety of materials was investigated. Although the above theories predict the experimental data astonishingly well they give no insight into the mechanism of melting.

The melting process has also been related to the spontaneous generation of dislocation dipoles [11]. After completion of the melting transition the dislocation cores are contiguous and long range order has vanished.

Computer simulations by Cotterill et al. [12,13] of the dislocation model permit the investigation of the time evolution of the phase transition in the range of some tens of vibrational periods ($\approx 10^{-10}$ seconds of real time). In later work the role of the surface was taken into account [14]. The melting process begins at the surface at a depressed temperature. The dislocation model gives reasonable values for the changes at the melting point of the diffusion constant, the electrical resistivity and the viscosity [12].

There are also experiments on two dimensional systems e.g. the melting of a monolayer film of butadiene iron tricarbonyl molecules adsorbed on graphite surfaces has been investigated by means of Mössbauer spectrometry [15]. The Debye-Waller factor for motion parallel to the surface decreases abruptly at a reproducible temperature, indicating a first order melting transition.

The bulk liquid has been investigated for prefreezing effects. The x-ray diffraction patterns of molten copper and lead can be explained by a paracrystalline structure of the liquid

even far above the melting point [16,17]. Light scattering experiments on CCl_4 show an increase in the total intensity of the light scattered from the liquid once the phase boundary approaches the scattering volume [18]. Supercooled water has been studied by Brillouin scattering [19]. In the supercooled regime the sound velocity decreases with decreasing temperature faster than it does above $0^{o}C$.

The solid-liquid phase transition is of the first order and involves latent heat and nucleation. Therefore, during crystal growth there is always an energy flow away from the interface. Because a nucleation energy is necessary for the creation of a crystal surface in the melt supercooling of the liquid is possible. However, for melting at the surface of a crystal in equilibrium with its vapor such a barrier does not exist because the solid-vapor surface tension is larger than (or equal to) the sum of the solid-liquid and the liquid-vapor surface tension [20]. The fact that all experimental attempts to superheat a whole crystal failed supports this view. Internal heating in crystals indicates that the creation of internal surfaces might involve a nucleation process [21]. Once the interface is created the transition occurs there.We do not know a realistic theory that takes into account both phases as well as the interface. However, the Ising model has been applied to the treatment

of the solid-liquid transition [22]. Space is divided into equal cells that are either solid ("spin up") or liquid ("spin down"). With the assumption that a cell can only solidify if it is on top of another solid cell the growth kinetics and the distribution of solid and liquid cells in the transition region have been calculated. In this model melting and solidification are strictly inverse.

The methods that have been applied until now to the observation of the dynamics of the interface have a limited time resolution (motion pictures). In the present work dynamic light scattering (light beating spectroscopy) is applied [23,24]. This method permits the observation of processes with a characteristic time as short as a microsecond. Spatial Fourier components above about 200 nm are accessible to investigation. This means that the observations are purely phenomenological.

Ice has been chosen because high purity single crystals with low dislocation density are available in the laboratory, because of its optical transparency and its convenient melting temperature.

2. EXPERIMENT

2.1 Experimental set-up

A block diagram of the experimental set-up is given in fig. 1. The sample and the photomultiplier are placed in a cold-room the temperature of which is stabilized at -18°C and fluctuates within less than 1°C. The laser (Spectra Physics 165 argon ion laser) and the correlator (MALVERN K7023) are outside. The laser beam passes through Brewster windows into the cold-room illuminating the interface under investigation in grazing incidence. The lens L1 (f = 10 cm) focuses the vertically polarized beam (TEM_{00}) to approximately 100 μm in diameter.

The scattered light is detected by a photomultiplier (EMI 9813KB). The preamplifier/discriminator as described in [25] is integrated into the PM-assembly. The dark count rate is held low (10 counts/s at -18°C and U = 1850 V) by magnetic defocusing. Increasing the high voltage of the photomultiplier above 1850 V causes self correlations in the dark current with a correlation time of about 1 μs. The photomultiplier is operated at 1850 V in order to avoid distortions of the photon correlation function. The PM-assembly is mounted on a turntable that permits the selection of the scattering angle. Measurements have been done between 10° and 140°.

The optics in front of the photomultiplier is shown in fig. 2. The lens L2 projects a real picture of the scattering region onto the adjustable rectangular aperture A2 (horizontal $\simeq$ 0,1 mm, vertical $\simeq$ 0,5 mm) that selects the scattering volume. The whole scattering region can be observed through the telescope L2, M, O by placing the mirror M into the light path. The vertical slit A1 ($\simeq$ 0,1 mm x 5 mm) determines the angular spread $\delta\Theta$ of the collecting system. L3 focuses the light through the magnet onto the cathode of the photomultiplier.

The optical axis of the PM-assembly is tilted by 1-2^{o} with respect to the basal plane. The incident beam is not exactly parallel to the basal plane but grazes the interface at an angle of about 1-2^{o}. The difference between the azimuthal angle Θ and the scattering angle can be neglected.

The digital 96-channel correlator calculates the real time single clipped autocorrelation function [24,26] of the number of counts arriving from the PM-assembly

$$G_{sc}^{(2)}(\tau;\Delta t) = \langle n(t;\Delta t)\, n_k(t+\tau;\Delta t)\rangle \,. \qquad (2.1)$$

The angular brackets denote a time average. $n(t;\Delta t)$ is the number of counts in the sample time interval of the length Δt

that begins at the time $t - \Delta t/2$. The clipped count rate $n_k(t; \Delta t)$ is defined by

$$n_k(t;\Delta t) = \begin{cases} 1 & \text{if } n(t; \Delta t) > k \\ 0 & \text{if } n(t; \Delta t) \leq k \ . \end{cases} \qquad (2.2)$$

It has been shown by Jakeman [26] that for Gaussian light

$$G_{sc}^{(2)}(\tau) \propto G^{(2)}(\tau) = \langle I(t)\ I(t+\tau)\rangle \qquad (2.3)$$

(where $I(t)$ is the intensity of the scattered light). For Gaussian light first and second order correlation functions are connected by the Siegert relation [26,27]

$$g^{(2)}(\tau) = 1 + \left|g^{(1)}(\tau)\right|^2 \qquad (2.3)$$

where $g^{(1)}(\tau)$ and $g^{(2)}(\tau)$ are the normalized field and intensity autocorrelation functions, respectively. The power spectrum is the Fourier transform of the field autocorrelation function.

The correlation function $G_{sc}^{(2)}(\tau)$ is monitored by an oscilloscope and punched on paper tape. These raw data are processed by a mini-computer (NOVA 3/12, Data General).

2.2 Preparation of the interface

a) Preparation of the seed crystals

The growth techniques for large ice single crystals have been developed in our laboratory [28]. Tubes of acrylic glass with a diameter of 95 mm and a length of about 600 mm are used for the zone refining. They are cleaned with a laboratory detergent and then rinsed with deionized water for several days. Rinsing is continued with water from a "Millipore" filter system consisting of a combination of an organic adsorption filter, an ion exchanger and a mechanical filter with a 0,22 µm Millitube cartridge. The water is circulated through the growth tube. When the conductance of the water in the tube is below $10^{-7}\ \Omega^{-1}cm^{-1}$ at $25^{o}C$, the tube is transferred to the cold-room. Provision is made that the water freezes slowly from the bottom to the top. The resulting polycrystal is transferred into a zone melting apparatus [28]. When the zone has passed the ice once a single cristalline region is formed by competitive growth and is used as a seed for the following zone refining passes. X-ray topography shows that the single crystals have a dislocation density of about $10^{3}\ cm^{-2}$ [28]. These crystals provide the material for the oriented seeds needed for our experiment.

The preparation of the seed starts from an ice cube that has been preoriented in c-direction by visual inspection of

epitactically grown frost crystals. The orientation is checked between crossed polaroids. Then the cube is frozen onto a goniometer mounted on a lathe in the cold-room such that the c-axis is approximately parallel to the lathe axis. Humidity from the surrounding air condenses as platelike epitactic frost crystals with an orientation $[1\bar{2}10]$ on the freshly cut cylinder surface. These frost crystals are illuminated with a HeNe-laser beam, oriented at a right angle to the lathe axis. The orientation of the seed crystal is adjusted by means of autocollimation of the laser beam on the frost crystals. The sample is then machined again so that the cylinder axis is parallel to c. The orientation error is less than 1^{o}.

b) Preparation of the sample

The seed is then transferred to the acryl glass tube used in the light scattering experiment (inner diameter 36 mm, length 400 mm) and frozen onto its stainless steel bottom. The remainder of the tube is filled with deionized water prepared as described above. Zone refining begins after solidification from the bottom to the top. After each pass the liquid dirty end is poured off and replaced by clean water. About 15 zone refining passes at a growth rate of 2 cm/d are completed before the single crystal is used in the light scattering experiment.

c) Formation of the interface

At the beginning of a run all the water is in the form of a single crystal. The tube is transferred to the zone melting apparatus which is part of the light scattering set-up. There it is partially (see fig. 3) immersed into two separately thermostated immiscible fluids. The upper liquid is silicone oil. It is heated above $0^{o}C$ by two independent loops in which a thermostated liquid is circulated. The lower liquid (cooling bath) is a mixture of methanol and aethylene glycol. It is cooled below the ambient temperature by two cooling loops connected to a third thermostat. The temperature of the circulating liquid can be lowered down to $-30^{o}C$.

Overnight a zone is molten into the lower part of the ice crystal (where it is of highest purity). An upward bulge of the lower interface is obtained by adjusting the temperatures of the heating- and cooling-coils at about $3^{o}C$ and $-6^{o}C$, respectively. The absence of dust in the interfacial region can be tested with the (488 nm) laser beam. The following criteria must be fullfilled in order to obtain reproducible results:

1. Absence of dust in the water

a) The focused beam (200 mW) in the water appears to be reddish which means that the Rayleigh and Brillouin-intensities together are lower than the intensity of the Raman scattering.

b) In foreward direction ($\Theta \simeq 20^{\circ}$) no dust particles are visible in the unfocussed beam.

2. Perfection of the ice surface

a) No bright spots are seen if the focused beam is totally reflected at the basal plane.

b) No small angle grain boundary groves are visible near the center of the crystal.

3. Homogeneity of the bulk ice

The ice is pure without inclusions. Only Raman scattering is visible.

After these tests the growth is initiated by lowering the growth tube into the cooling bath ($-15^{\circ}C$) with a speed of $v \simeq 0{,}6$ µm/s. A few hours later a basal plane ([0001]-face) is formed at the top of the growing crystal. Then the growth rate is increased by continuously lowering the temperature of the cooling bath down to $-28^{\circ}C$. The diameter of the basal plane increases up to about half the tube diameter. The rate at which the crystal is lowered is adjusted to the instantaneous growth rate, so that the basal plane does not move with respect to the optical system. The crystal is now ready for the light scattering experiment.

To prevent convection in the molten zone the temperature of the two heating thermostats must not exceed $4^{\circ}C$. Hence at high

growth rates it is not possible to melt as much ice on top of the zone as water is frozen at the cold end. Therefore the gap between the solid phases closes during the experiment, limiting its duration to 2 to 5 hours.

2.3 Dependence of the scattering intensity on the growth rate

At low growth rates no light scattering at the interface was observed that exceeded significantly the background arising from the bulk water even if the crystal had grown for several hours. Light scattering was observed only if the critical growth velocity v_{crit} = 1,5 µm/s was exceeded. Fig. 4 shows the dependence of the scattering intensity on the growth rate in the range from 0,03 µm/s to 2,5 µm/s. At $v > v_{crit}$ light scattering was observed to start at a spot on the basal plane. It took about half an hour for this scattering region to spread out over the basal plane. During this period the luminosity of the scattering region increased. A spot was selected for observation where the scattering was uniform without bright points in the neighborhood. The increase of the scattering intensity is a transient and was observed only qualitatively. If one stabilized the growth rate at a value above v_{crit} the scattering intensity became independent of time. At decreasing growth rate it did not drop to the background value at v_{crit} but decreased linearly with the growth

rate. After melting the crystal surface no scattering could be observed until the growth rate had again exceeded v_{crit}. This hysteresis behavior was found for all samples *). Usually the laser beam was blocked before the onset of scattering except for short periods where laser light was needed for visual observation. Dynamic scattering was discriminated against Raman, Brillouin and static scattering by means of the photon correlation. Scattering was visible in the interface region only. It was never observed during melting. It is, however, important to note that the realizable melting velocities were considerably below v_{crit}.

2.4 Dependence of the scattering intensity on the incident laser power

For an estimation of the influence of laser heating on the scattering process the dependence of the intensity of the scattered light on the power of the incident laser beam was measured. The results are shown in fig. 5 for growth rates

---

*) The hysteresis was also observed at the interface of a crystal with its c-axis oriented perpendicular to the growth direction. Scattering occured at the highest point of the convex shaped crystal. The threshold growth velocity was about the same.

of 1,9 μm/s and 0,73 μm/s. No deviations from a linear behavior occured for laser powers up to 400 mW. Most of the experiments were performed at 200 mW. Thus we may assume that laser induced heating does not affect the scatterers.

For an estimate of the temperature rise due to absorption of laser light in bulk water we assume a Gaussian intensity distribution in the cross section of the laser beam. For an infinite aperture one can write

$$I(r) = I_0 \exp\ (-2r^2/w_0^2) \qquad (2.5)$$

where w_0 is the characteristic radius of the beam. The steady state heat flow equation that governs the temperature distribution $\theta(r)$ around the laser beam is

$$-k_w 2\pi r\ \frac{\partial\theta}{\partial r} = \int_0^r 2\pi r'\ \beta I_0 \exp\left(\frac{-2r'^2}{w_0^2}\right) dr' \qquad (2.6)$$

where k_w is the thermal conductivity of water and β designates the absorptivity of water. $\theta(r)$ is the deviation from the temperature that prevails at a distance $r_0 >> w_0$ from the beam axis. On the beam axis one obtains approximately [29]

$$\theta(r=o) \simeq \frac{0{,}06\ \beta I_0}{k_w}\ \ln\left(\frac{2\ \gamma r_0^2}{w_0^2}\right) \qquad (2.7)$$

with $\gamma = 1{,}781....$ For $\beta = 2{,}1\cdot10^{-2}m^{-1}$ [30], $I_0 = 0{,}2$ W, $w_0 = 50$ μm and $r_0 = 1$ cm one obtains $\theta(r=o) = 5{,}3$ mK.

This value may be considered an upper limit because in our experiment the scattering volume is directly above the ice which is a better heat conductor than water by a factor of four. Possible heating effects in the ice due to the evanescent wave were neglected. The thus calculated temperature rise is much smaller than the supercooling at the interface ($7 \cdot 10^{-2}$°C for v = 1 µm/s, see appendix A). This is compatible with the observation that the laser induced heating does not affect the scattering process.

2.5 Angular dependence of the scattering intensity

The accuracy of the measurement of the angular dependence of the scattering intensity was impaired because it was difficult to ascertain that exactly the same spot on the basal plane was observed after a change of the scattering angle. In addition there was some stray light from the glass walls. For the measurement the optical arrangement (see fig. 2) was modified by replacing the variable aperture A2 by a pinhole of 300 µm in diameter. Fig. 6 shows that there is no angular dependence within the rather large experimental error. The data are corrected for the angular dependence of the scattering volume

$$I_{corr}(\Theta) = I_{meas}(\Theta) \sin \Theta \, . \qquad (2.8)$$

2.6 Linewidth measurements

The following observations have been made:

1) The dynamical scattering observed with our equipment occurs in a thin layer at the interface only.

The small scattering intensities of bulk water or ice showed no dependence of the correlation function upon the parameter τ within the angular range and the time resolution accessible to our equipment. The analysis of the scattered light from the acryl glass revealed that there were no vibrations in the apparatus.

2) Within experimental error the measured correlation function can be fitted by a single exponential.

A typical correlation function (by far not the best) is shown in fig. 7. The interruptions in the curve at high delay times are due to the insertion of additional delays in the shift register of the correlator. This expansion of the time scale permits a more accurate determination of the base line. The fitting function is

$$G_{sc}^{(2)}(\tau) = A + B \cdot \exp\left(-\frac{2\tau}{C}\right) . \qquad (2.9)$$

The data reduction was performed using a nonlinear least squares fitting procedure [31]. No weighting was introduced.

The quality of the fit is illustrated by the semi-logarithmic plot in fig. 8.

3) The following observations indicate that our measurements have to be interpreted assuming self beat detection.

According to theory the ratio B/A in eq. (2.9) for pure self beat detection and Gaussian light has an upper bound of 1 [26]. If heterodyne detection would dominate one would have $B/A << 1$. We obtained values up to 0.5 (not corrected for spatial and temporal integration, see section 2.7).

4) We do not observe fluctuations that are due to scatterers entering and leaving the scattering volume. These so called number-fluctuations would increase the background.

The base line of the fitting function eq. (2.9) can be calculated independently of the fit using the data stored in the monitor channels of the correlator [32]. Therefore one can check the data for excess background [33,34]. We found agreement between the two base lines within 1 % of B.

5) The measured linewidth is proportional to the square of the scattering vector.

Fig. 9 shows the results for two crystals. The straight lines are least squares fits to the experimental data. For crystal #2 the straight lines for two different growth rates agree within the scatter of the data. The reproducibility of the slope is within about ± 20% from run to run. Crystal #2 showed (over about 10 runs) somewhat higher values of the linewidth than crystal #4.

The linewidth measurement was reproducible within 100 rad/s over a period of some minutes (a measurement at $\Theta = 90^{\circ}$ takes about 50 seconds). The scatter of the data became larger (see fig. 9) if the scattering angle was changed between measurements, for reasons pointed out earlier. In addition to these spatial variations of the scattering properties they may vary somewhat with time (see fig. 10). The uncertainty of the scattering angle has negligible influence on the Γ versus K^2 plots. By measurements in which the Malvern correlator in the clipping mode and a full correlator were used simultaneously it was checked whether the clipping has an influence on the resulting linewidth. No difference was found.

6) The linewidth is independent of growth rate.

The data in fig. 10 are from the same run with crystal #2

as the data plotted in fig. 9. First the crystal was brought to a growth rate of 1,6 μm/s. During an hour this velocity was kept constant while the data shown in fig. 9 were taken. Then the growth rate was reduced by increasing the temperature of the cooling bath. The linewidth remained constant within experimental scatter down to a growth rate of 0,03 μm/s. Below this speed the ratio B/A (see eq. 2.9) became so small that the time needed for the accumulation of acceptable data became prohibitive.

7) The change of the crystal orientation (rotation around the c-axis) does not affect the linewidth within experimental error. The six fold crystal symmetry does not manifest itself.

8) At a scattering angle of $\Theta = 90^{\circ}$ no depolarized component in the scattered light was found. If the polarization was rotated by 90° so that the electrical field was parallel to the basal plane the scattering intensity vanished at $\Theta = 90^{\circ}$.

9) In an exploratory experiment the light scattered in the direction perpendicular to the basal plane was analyzed. Within experimental error the linewidth was found to be

the same as for 90^{o}-scattering in the basal plane at a growth rate of v = 2,1 μm/s. The scattering intensity vanishes for vertical polarization of the incident light.

2.7 Estimate of the thickness of the scattering region

The linear dimensions of the scattering region can be determined by measuring the spatial coherence properties of the scattered light. Jakeman et al. have quantitatively analyzed this effect for circular apertures [35]. According to general theory one has for Gaussian light and self beat detection $\frac{B}{A} \leq 1$ [26], where the limit 1 corresponds to a detector area infinitely small compared to a coherence area. In an actual experiment this condition is not fulfilled and, moreover, the correlation function is integrated over time intervals of the length Δt, the sampling time set at the correlator. Under these conditions the Siegert relation eq. (2.4) has to be modified slightly to [26],

$$g_{sc}^{(2)}(\tau;\ \Delta t,\ k, \mathcal{A}) \simeq 1 + f_1(\Delta t) f_2(k) f_3(\mathcal{A}) / g^{(1)}(\tau) /^2 \qquad (2.10)$$

where $\mathcal{A}$ is the detector area, k the clipping level and (see eq. (2.9))

$$f_1(\Delta t) f_2(k) f_3(\mathcal{A}) = B/A. \qquad (2.11)$$

$f_1(\Delta t)$ is approximately unity if the sampling time Δt is short compared to the correlation time $\tau_c = \frac{1}{\Gamma}$. According to reference [26] one has

$$f_2(k) = \frac{1 + k}{1 + \langle n(t) \rangle} \quad , \tag{2.12}$$

which is exact in the absence of temporal and spatial integration *). In order to keep $f_2(k)$ close to unity one choses $k \simeq \langle n(t) \rangle$ in the experiment. Then

$$B/A \simeq f_3(\mathcal{A}) \quad . \tag{2.13}$$

A simple hypothetical arrangement for the measurement of the coherence properties of the scattered light is shown in fig. 11. The source is located in a plane parallel to the yz-plane. The aperture $\mathcal{A}$ determines the detector area. The distance between the scattering volume and $\mathcal{A}$ is designated by x_0. The degree of spatial coherence of the scattered light in the far field is given by [37,38]

$$/\gamma^{(1)}(y,z;y',z')/ = \left| \frac{\sin \kappa_y/y-y'/}{\kappa_y/y-y'/} \quad \frac{\sin \kappa_z/z-z'/}{\kappa_z/z-z'/} \right| \tag{2.14}$$

$$\kappa_y = \frac{2\pi\, s_y}{\lambda \cdot x_0} \quad , \quad \kappa_z = \frac{2\pi\, s_z}{\lambda \cdot x_0} \quad . \tag{2.15}$$

---

*) This point was carefully checked using a Latex solution. Our results were later confirmed by other authors [36].

The function $f_3(\mathcal{A})$ is obtained by integration over the aperture $\mathcal{A}$ [35]

$$f_3(\mathcal{A}) = \frac{1}{\mathcal{A}^2} \int_{\mathcal{A}} dydz \int_{\mathcal{A}} dy'dz' / \gamma^{(1)}(y,z;y',z') /^2 . \quad (2.16)$$

If a narrow vertical slit of height $2L_z$ is used for $\mathcal{A}$ the y-term in eq. (2.14) is very close to unity and eq. (2.16) reduces to

$$f_3(\mathcal{A}) \simeq f_3(L_z) = \frac{1}{(2L_z)^2} \int_{-L_z}^{L_z} dz \int_{-L_z}^{L_z} dz' \left(\frac{\sin \kappa_z/z-z'/}{\kappa_z/z-z'/}\right)^2 . \quad (2.17)$$

This function is plotted in fig. 12.

The geometry of the actually used optical arrangement (see fig. 2) is too complicated to permit the exact calculation of the dimensions of the effective scattering volume. However, its thickness can be estimated using the measured ratio B/A. The slit height $2L_z$ of the aperture A1 of the PM-assembly could be adjusted in the range between 0 and 5 mm. The distance between the scattering volume and the aperture A1 was $x_0 \simeq 83$ mm. Fig. 13 shows the measured B/A values for $\Theta = 90^\circ$ as a function of L_z not only for ice (where the thickness of the scattering volume is unknown) but also for a Latex solution (where the diameter of the scattering volume is equal to the known beam diameter). The optical arrangement

was identical in both cases. These experimental data were compared to the calculated function $f_3(L_z)$ represented in fig. 12. For Latex one arrives at a beam diameter of roughly $2s_z$ = 60 µm, which agrees with the diameter calculated by means of diffraction theory. For ice B/A decreases only slightly with increasing L_z. At $2L_z$ = 5 mm $\kappa_z L_z$ is still smaller than unity. As an estimate for the vertical dimension of the projection of the scattering volume one obtains $2\ s_z \simeq 6\mu m$. The main contribution to this value is due to the fact that s_z is a function of z because the scattering volume extends over about 100 µm in x-direction. Therefore $2\ s_z$ is only an upper limit for the thickness of the scattering layer.

2.8 Early experiments with an interface prepared by the Kyropoulos method

In the early experiments [39] a different arrangement had been used. An icicle grew into thermostated water. The water was in contact with laboratory air and thus contamination with dust particles and carbon dioxide was hard to prevent. The data reduction showed clearly that there was more than one exponential in the photon correlation function. Two decay times ("slow" and "fast" component) were fitted. In the light of the perfected experiment one can ascribe the slow component to dust whereas the fast component corresponds

to the measurements reported in section 2.6. Since the scattering from the ice (see fig. 4) becomes stronger with increasing growth rate the fit made both components to appear faster at high growth rates. Thus, at large scattering angles and high growth rates the fast component originating from the ice had been dominant. The value of 3 krad/s at $\Theta = 180^{o}$ is not far from the results described in section 2.6 for crystal #4.

3. ATTEMPTS OF AN INTERPRETATION

We restrict ourselves to an interpretation of the linewidth of the scattered light. The hysteresis behavior of the scattering intensity versus growth rate and the threshold of the growth rate are subject of further studies.

First we rule out the possibility that the scattering is due to ice clusters that undergo Brownian motion in the supercooled water in front of the interface. Then we consider fluctuations of the interface.

3.1 Diffusing clusters

It is well known that the light scattered from a dilute suspension of monodisperse spherical clusters undergoing Brownian motion shows a Rayleigh-linewidth proportional to the square of the scattering vector [40]

$$\Gamma = D_T K^2 \quad . \tag{3.1}$$

From the experimental results for crystal #2 in fig. 9 a translational diffusion constant $D_T = 0{,}4 \cdot 10^{-7} \frac{cm^2}{sec}$ is obtained. The Stokes-Einstein relation

$$r = \frac{k_B T}{\pi \eta D_T} \tag{3.2}$$

yields a hydrodynamic radius $r = 25$ nm. k_B is the Boltzmann constant and η the viscosity of the water.

An ice cluster in water decays if its radius is smaller than a critical radius given by

$$r^* = \frac{2\,\sigma_{SL}}{\Delta S_f\,\Delta T} \qquad (3.3)$$

(see appendix C and [4]). σ_{SL} is the surface tension between water and ice, ΔS_f is the entropy of fusion and

$$\Delta T = T_m - T_w \qquad (3.4)$$

is the supercooling of the water. T_m is the melting temperature of a flat interface and T_w is the actual temperature of the water near the interface. The work necessary for the creation of a cluster with $r = 25$ nm at the supercooling $\Delta T = 0{,}1^{\circ}C$ (corresponding to the growth rate of 2,6 µm/s) is

$$W = -\frac{4\pi}{3}\, r^3\, \Delta S_f\, \Delta T + 4\,\pi r^2\, \sigma_{SL} = 2{,}36 \cdot 10^{-16}\ J. \qquad (3.5)$$

The probability for the creation of such a cluster by thermal fluctuations contains the prohibitive factor

$$e^{-W\,/\,k_B T} = e^{-6{,}1\cdot 10^4}\ . \qquad (3.6)$$

Furthermore one cannot understand why diffusing clusters should be confined to a layer of a few microns.

3.2 Interface fluctuations

This purely phenomenological model describes the dynamics of the deviations of the interface from a flat surface. We introduce the following frames of reference (see fig. 14).

xyz is attached to the lattice of the growing crystal. z is parallel to the growth direction.

x'y'z' moves with the constant macroscopic growth velocity v along z. The x'y'-plane is the "mean basal plane".

The equation of the actual interface shall be given by $z' = \zeta(x',y',t)$. The local velocity of the interface in the unprimed system is assumed to be proportional to the difference between the chemical potentials of ice and water. We write

$$\frac{\partial \zeta}{\partial t} + v = \alpha \Delta\mu \ , \qquad (3.7)$$

where α is a constant. The linear dependence of v on $\Delta\mu$ for a macroscopically flat surface has been verified experimentally [41] for ice growing in the direction of the basal plane for growth rates up to $\pm 0{,}1\ \mu m/s$.

The temperature of the water is $T_w = T_m - \Delta T$ (see eq. (3.4)). The difference between the chemical potentials of liquid and solid can then be written as

$$\Delta\mu = \mu_i (p_w + \delta p, T_m - \Delta T) - \mu_w (p_w, T_m - \Delta T). \quad (3.8)$$

The suffixes i and w designate the ice and the water, respectively. $\delta p = p_i - p_w$ is the local pressure difference at a curved interface between ice and water due to surface tension. δp is given by the Laplace formula [42]. For small curvature one has

$$\delta p \simeq - \sigma_{SL} \vec{\nabla}_S^2 \zeta \quad (3.9)$$

where $$\vec{\nabla}_S = \frac{\partial}{\partial x} \vec{i} + \frac{\partial}{\partial y} \vec{j} .$$

With $d\mu = -s\, dT + v\, dp$ one obtains from eq. (3.8)

$$\Delta\mu = (s_i - s_w) \Delta T + v_i \delta p. \quad (3.10)$$

$s_i - s_w$ is the entropy of fusion for a single water molecule. v_i is the volume occupied by a molecule in the ice. The first term in eq. (3.10) is always nonzero for a growing crystal. The second term is the contribution of curvature.

Inserting eq. (3.10) and (3.9) into eq. (3.7) one has

$$\frac{\partial \zeta}{\partial t} + v = \alpha (s_i - s_w) \Delta T - \alpha v_i \sigma_{SL} \vec{\nabla}_S^2 \zeta . \quad (3.11)$$

For a flat surface the terms with ζ vanish and eq. (3.11) can be compared with the empirical relation $v = \mu_T \Delta T$ (3.12) discussed in appendix A. The result is

$$\alpha = \frac{\mu_T}{s_i - s_w} = - \frac{\mu_T}{\Delta S_f \, v_i} \quad . \tag{3.13}$$

Therefore we obtain in the moving coordinate system x'y'z'

$$\frac{\partial \zeta}{\partial t} = \frac{\mu_T \, \sigma_{SL}}{\Delta S_f} \vec{\nabla}_S^2 \, \zeta \quad . \tag{3.14}$$

This equation describes the decay of the interface fluctuations.

3.3 Light scattering from interface fluctuations

Mandelstam and coworkers have calculated the intensity of the light scattered by a corrugated interface [43,44] . They considered thermal fluctuations of the surface of a liquid. The dynamics of these fluctuations was measured by Katyl and Ingard [45] and Bouchiat and Meunier [46,47]. In all this work the amplitudes of the Fourier components of the fluctuations were small compared to the wavelength. For fluctuations of the ice-water interface, however, this is not necessarily true. Therefore the formalism developped for the fluctuations of a liquid surface cannot be applied to our case without further considerations, unless the scattering plane is the x'y' plane. The first order correlation function is then given by

$$g^{(1)}(\tau) \propto < \zeta(\vec{K},t) \; \zeta \; (\vec{K}, \; t+\tau) > \quad . \tag{3.15}$$

The transformation of eq. (3.14) into $\vec{K}$-space immediately yields an exponential decay with the decay rate

$$\Gamma = \frac{\mu_T \sigma_{SL} K^2}{-\Delta S_f} \quad , \text{ where } K^2 = K_x^2 + K_y^2 . \tag{3.16}$$

With

$$\zeta(\vec{K}, t+\tau) = \zeta(\vec{K},t)\, e^{-\Gamma\tau} \tag{3.17}$$

one has then

$$g^{(1)}(\tau) \propto < |\zeta(\vec{K},t)|^2 > e^{-\Gamma\tau} \quad . \tag{3.18}$$

Inserting the empirical values
$\mu_T = 10^{-4}\ ms^{-1}\ K^{-1}$, $\sigma_{SL} = 3 \cdot 10^{-2}\ Jm^{-2}$ and
$\Delta S_f = 1{,}12 \cdot 10^{6}\ Jm^{-3}\ K^{-1}$ (see appendices A,B,D) one obtains for $\Theta = 90^{\circ}$ and $\lambda = 488$ nm the value $\Gamma = 1580$ rad/s. The agreement with the experiment is surprising, in particular, if one considers the linear approximation made for the growth rate as a function of supercooling.

The interpretation of the observation #9 in section 2.6 requires further experimental and theoretical work. It is to be expected that the width of the Rayleigh line depends not only upon the decay time τ_c of the amplitude of the fluctuations but also upon the amplitude itself and hence on the growth rate.

4. APPENDIX

A. Growth kinetics of ice

The kinetics of freezing of ice in the direction perpendicular to the basal plane has been measured by Hillig [48]. The experiments were made in thin walled glass capillaries placed in a refrigerated bath of constant temperature. The speed v of the solid-liquid interface was observed as a function of the supercooling ΔT at the interface. Since the phase boundary is a heat source $T_m - \Delta T$ is slightly higher than the bath temperature. Hillig corrected for this effect. Although this heat-dissipation analysis has been criticized in part by Michaels et al. [49] the data of the two authors agree quite well. $v(\Delta T)$ is given in fig. 15.

The theory in section 3.2 is based on the assumption of a linear approximation for the growth kinetics in the range $-100\ \mu m/s < v < 100\ \mu m/s$. Hillig finds a difference between perfect and imperfect crystals. Since our light scattering experiments indicate a corrugated interface it is reasonable to use the data for imperfect crystals which can be expressed by the relation [50]

$$v = 1 \cdot 10^{-4} \ \Delta T^{1,23} \quad [m/s] \quad .$$

We approximate this by

$$v = \mu_T \ \Delta T \quad \text{with} \quad \mu_T = 10^{-4} \ \frac{m}{sK}$$

and assume moreover that this relation is not only valid for solidification but also for melting.

B. Surface tension of the interface ice-water

Table 1 summarizes some measurements of the solid-liquid interfacial free energy σ_{SL}. Measurements of the nucleation rate vs. temperature are indirect because they require extrapolation from the nucleation temperature to the melting point. Moreover, the shape of the nucleus is usually assumed to be spherical. A very direct method is discussed in the paper by Hardy [51]. The experimentally observed shape of a grain boundary groove is fitted to its theoretically predicted shape. This method yields a precise value for σ_{SL} both for equilibrium and dynamic conditions. The anisotropy of σ_{SL} is small [52]. In the calculation in section 3.3 we insert the value $\sigma_{SL} = 30\ mJ/m^2$.

Author		Ref.	σ_{SL} [mJm^{-2}]	T[°C]	method
Fisher et al.	1949	53	32,8		HN
Jacobi	1955	54	24	0	HN
			15,1	-40	
Skapski et al.	1957	55	44±10	0	CC
Kuhns et al.	1968	56	20		HN
Ketcham and Hobbs	1969	52	33±3	0	DAC
Jones	1970	57	26,1		
Wood and Walton	1970	58	31,93±0,44	0	HN
			24,22±0,02	-36,55	
Coriell et al.	1971	59	25±2	≃0	IP
Jones	1973	60	44±10	0	GBG
Jones	1974	57	46		
Hardy	1977	51	29,1±0,8	0	GBG

Table 1

C. Equilibrium conditions for the liquid-solid interface of a small cluster

The system is composed of three parts:

Liquid phase

T_0 Temperature

p_0 Pressure

V_0 Volume

N_0 Number of molecules

Solid phase

T_1, p_1, V_1, N_1

Interface (surface of V_1)

T_2 Temperature

O Area

The energy of the system is:

$$\begin{aligned} U &= U_0 + U_1 + U_2 \\ &= T_0S_0 - p_0V_0 + \mu_0N_0 \\ &\quad + T_1S_1 - p_1V_1 + \mu_1N_1 \\ &\quad + T_2S_2 + \Sigma \,. \end{aligned}$$

S_i are the entropies and $\Sigma = \sigma_{SL}O$ ist the surface free energy. σ_{SL} is the interfacial free energy per unit area, assumed to be a function of temperature only.

U is to be minimal under the following conditions:

a) $S = S_0 + S_1 + S_2 = \text{const.}$

b) $N = N_0 + N_1 = \text{const.}$

c) $V = V_0 + V_1 = \text{const.}$ (with the assumption $V_0 >> V_1$) .

For positive σ_{SL} Σ is minimal if V_1 has sperical shape. Thus, with $O = 4\pi r^2$, $V_1 = \frac{4\pi}{3} r^3$, $dO = \frac{2}{r} dV_1$ and

$$dU = T_0 dS_0 - p_0 dV_0 + \mu_0 dN_0 + T_1 dS_1 - p_1 dV_1 + \mu_1 dN_1 + T_2 dS_2 + \sigma dO$$

the conditions a) to c) yield:

a) $T_0 = T_1 = T_2 = T = \frac{\partial U}{\partial S}$

b) $dN_1 = -dN_0$, $\mu_0 = \mu_1 = \mu = \frac{\partial U}{\partial N}$

c) $dV_1 = -dV_0$, $p_0 = p_1 - \frac{2\,\sigma_{SL}}{r}$.

r is the radius of the cluster and $\frac{2\,\sigma_{SL}}{r}$ the pressure increase in V_1 due to surface tension. For a flat surface in equilibrium one has

$$\mu_1(p_0, T_m) = \mu_0 (p_0, T_m)$$

and for a curved surface

$$\mu_1(p_0 + \frac{2\,\sigma_{SL}}{r}, T_m - \delta T) = \mu_0(p_0, T_m - \delta T).$$

T_m is the melting temperature and $T_m - \delta T$ the equilibrium temperature for the curved interface. Subtracting the first equation from the second one obtains with $d\mu = - sdT + vdp$

$$s_l \delta T + v_l \frac{2\sigma_{SL}}{r} = s_0 \delta T$$

$$\delta T = \frac{2\sigma_{SL} v_l}{(s_0 - s_l) r} = \frac{2\sigma_{SL}}{\Delta S_f r} \quad . \qquad (A.1)$$

s_i and v_i are the entropies and volumes per molecule. The Gibbs-Thomson equation (A.1) gives the temperature difference δT necessary to keep a cluster of radius r in unstable equilibrium with the liquid. Such a cluster is often called a critical nucleus because clusters bigger than r_{crit} grow at a given undercooling δT.

D. Some physical constants of water and ice at $0^{\circ}C$

a) Water

density	$\rho_w = 999,84$	$kg\ m^{-3}$	[61]
specific heat	$Cp_w = 4,2177 \cdot 10^3$	$Jkg^{-1}\ K^{-1}$	[62]
thermal conductivity	$k_w = 0,561$	$Wm^{-1}\ K^{-1}$	[62]
index of refraction (λ=486 nm)	$n_w = 1,3380$		[63]
absorptivity (λ=488 nm)	$\beta = 0,021$	m^{-1}	[30]
viscosity	$\eta = 1,798 \cdot 10^{-3}$	$Ns\ m^{-2}$	[62]

b) Ice

density	$\rho_i = 916,71$	$kg\ m^{-3}$	[61]
specific heat ($-2^{\circ}C$)	$Cp_i = 2,101 \cdot 10^3$	$Jkg^{-1}\ K^{-1}$	[62]
thermal conductivity	$k_i = 2,2$	$Wm^{-1}\ K^{-1}$	[51]
index of refraction	$n \simeq 1,31$		[64]
melting temperature	$T_m = 273,15$	K	[61]
latent heat of fusion	$L_v = 3,05 \cdot 10^8$	Jm^{-3}	[51]
entropy of fusion	$\Delta S_f = L_v/T_m = 1,117 \cdot 10^6$	$JM^{-3}K^{-1}$	

5. REFERENCES

1. Coriell S.R., Sekerka R.F., J.Crystal Growth 34, 157 (1976)

2. Langer J.S., Turski L.A., Acta Metall. 25, 1113 (1977)

3. Langer J.S., Acta Metall. 25, 1121 (1977)

4. Woodruff D.P., "The Solid-Liquid Interface", Cambridge University Press, London (1973)

5. Fritsch G. in "Anharmonic Lattices, Structural Transitions and Melting" edited by T. Riste, Noordhoff, Leiden (1974) , p. 441

6. Adlhart W., Fritsch G., Lüscher E., Phys.Lett. 48A, 239 (1974)

7. Lindemann F.A., Physik.Zeits. 11, 609 (1910)

8. Born M., J.Chem.Phys. 7, 591 (1939)

9. Brillouin L., Phys.Rev. 54, 916 (1938)

10. Reynolds P.A., J.Phys.C: Solid State Phys. 10, 4449 (1977)

11. Kuhlmann-Wilsdorf D., Phys.Rev. A 140, 1599 (1965)

12. Cotterill R.M., Jensen E.J., Kristensen W.D. in "Anharmonic Lattices, Structural Transitions and Melting" edited by T. Riste, Noordhoff, Leiden (1974) p. 405

13. Cotterill R.M.J., Kristensen W.D., Jensen E.J., Phil.Mag. 30, 245 (1974)

14. Cotterill R.M.J., Phil.Mag. 32, 1283 (1975)

15. Shechter H., Suzanne J., Dash J.G., Phys.Rev.Lett. 37, 706 (1976)

16. Hosemann R., Willmann G., Roessler B., Phys.Rev.A 6, 2243 (1972)

17. Steffen B., Hosemann R., Phys.Rev. B 13, 3232 (1976)

18. Djabourov M., Lévy - Mannheim C., Leblond J., Papon P., J.Chem.Phys. 66, 5748 (1977)

19. Rouch J., Lai C.C., Chen S.H., J.Chem.Phys. 65, 4016 (1976)

20. Couchman P.R., Jesser W.A., Phil.Mag. 35, 787 (1977)

21. Käss M., Magun S., Z.Kristallographie 116, 354 (1961)

22. Pfeiffer H., Haubenreisser W., Klupsch T., Phys.Stat. Sol. (b) 83, 129 (1977)

23. Benedek G.B. in "Brandeis University Summer Institute in Theoretical Physics 1966; Statistical Physics, Phase Transitions and Superfluidity", edited by M. Chrétien, E.P. Gross and S. Deser, Vol. 2, 1, Gordon and Breach, New York (1968)

24. Chu B., "Laser Light Scattering", Academic Press, New York (1974)

25. Güttinger H., Gautschi M., Serrallach E., J.Phys.E: Sci.Instr. 9, 936 (1976)

26. Jakeman E., in "Photon Correlation and Light Beating Spectroscopy", edited by H.Z. Cummins and E.R. Pike, Plenum Press, New York (1974), p. 75

27. Glauber R.J., Phys.Rev. 131, 2766 (1963)

28. Bilgram J., Wenzl H., Mair G., J.Crystal Growth 20, 319 (1973)

29. Gordon J.P., Leite R.C.C., Moore R.S., Porto S.P.S., Whinnery J.R., J.Appl.Phys. 36, 3 (1965)

30. Hass M., Davisson J.W., J.Opt.Soc.Am. 67, 622 (1977)

31. Bevington P.R., "Data Reduction and Error Analysis for the Physical Sciences", Mc.Graw Hill, New York (1969)

32. Oliver C.J., in "Photon Correlation and Light Beating Spectroscopy", edited by H.Z. Cummins and E.R. Pike, Plenum Press, New York (1974), p. 151

33. Schaefer D.W., Berne B.J., Phys.Rev.Lett. 28, 475 (1972)

34. Pusey P.N. in "Photon Correlation Spectroscopy and Velocimetry" edited by H.Z. Cummins and E.R. Pike, Plenum Press, New York (1977), p. 45

35. Jakeman E., Oliver C.J., Pike E.R., J.Phys.A (gen. phys.) 3, L 45 (1970)

36. Nieuwenhuysen P., Clauwaert J., Rev.Sci.Instr. 48, 699 (1977)

37. Mandel L., Wolf E., Rev.mod.Phys. 37, 231 (1965)

38. Cummins H.Z., Swinny H.L., Progress in Optics 8, 133 (1970)

39. Güttinger H., Bilgram J.H., Serrallach E., Känzig W., Helvetica Physica Acta 48, 399 (1975)

40. Cummins H.Z., in "Photon Correlation and Light Beating Spectroscopy", edited by H.Z. Cummins and E.R. Pike, Plenum Press, New York (1974), p. 285

41. Miksch E.S., Rev.Sci.Instr. 36, 797 (1965)

42. Landau L.D., Lifshitz E.M., "Fluid Mechanics", Pergamon Press, London (1959)

43. Mandelstam L., Ann.Physik 41, 609 (1913)

44. Andronov A.A., Leontovich M.A., Z.Phys. 38, 485 (1926)

45. Katyl R.H., Ingard U., Phys.Rev.Lett. 20, 248 (1968)

46. Bouchiat M.A., Meunier J., J.de Phys. 32, 561 (1971)

47. Langevin D., Meunier J. in "Photon Correlation Spectroscopy and Velocimetry" edited by H.Z. Cummins and E.R. Pike, Plenum Press, New York (1977), p. 501

48. Hillig W.B. in "Growth and Perfection of Crystals" edited by R.H. Doremus, B.W. Roberts and D. Turnbull, John Wiley, New York (1958) p.350

49. Michaels A.S., Brian P.L.T., Sperry P.R., J.Appl.Phys. 37, 4649 (1966)

50. Cahn J.W., Hillig W.B., Sears G.W., Acta Metall. 12, 1421 (1964)

51. Hardy S.C., Phil.Mag. 35, 471 (1977)

52. Ketcham W.M., Hobbs P.V., Phil.Mag. 19, 1161 (1969)

53. Fisher J.C., Hollomon J.H., Turnbull D., Science 109, 168 (1949)

54. Jacobi W., Z.Naturforsch. 10a, 322 (1955)

55. Skapski A., Billups R., Rooney A., J.Chem.Phys. 26, 1350 (1957)

56. Kuhns I.E., Mason B.J., Proc.R.Soc. A 302, 437 (1968)

57. Jones D.R.H., J.Mat.Sci. 9, 1 (1974)

58. Wood G.R., Walton A.G., J.Appl.Phys. 41. 3027 (1970)

59. Coriell S.R., Hardy S.C., Sekerka R.F., J.Cryst.Growth 11, 53 (1971)

60. Jones D.R.H., Phil.Mag. 27, 569 (1973)

61. Eisenberg D., Kauzmann W., "The Structure and Properties of Water", Oxford University Press, London (1969)

62. Handbook of Chemistry and Physics, 56nd edition, The Chemical Rubber Press (1975)

63. Landolt-Börnstein, 8. Teil, Springer (1962)

64. Hobbs P.V., "Ice Physics", Clarendon Press, Oxford (1974)

Figure captions

1. Block diagram of the experiment.

2. Optics in front of the photomultiplier. L: lens, A: aperture, M: mirror, O: eyepiece, PM: photomultiplier, DM: defocusing magnet.

3. Zone melting apparatus.

4. Scattering intensity versus growth rate.

5. Scattering intensity as a function of the incident laser power for two different growth rates.

6. Angular dependence of the scattering intensity.

7. Intensity autocorrelation function as measured with the correlator (dots). The solid line is the least squares fit to a single exponential with floating base line. The horizontal line is the base line calculated from the monitor channels of the correlator.

8. Semi-logarithmic plot of the data of fig. 7.

9. Linewidth versus the square of the scattering vector for crystals #2 and 4. The straight lines are least squares fits.

10. Linewidth versus growth rate.

11. Optical arrangement for the quantitative measurement of the spatial coherence properties of a planar source.

12. Calculation of $f_3(L_z)$ as a function of $\kappa_z L_z$ (see eq. 2.17)

13. Coherence properties of the scattered light.
+ : reference measurement with Latex spheres;
Δ,o two runs with crystal #4.

14. Frames of reference.

15. Growth rate as a function of the supercooling at a macroscopically planar interface.

Table 1: Some measurements of the surface free energy of the water-ice interface. HN: homogeneous nucleation, CC: conical capillary, DAC: dihedral angles and contact angle, IP: interfacial perturbation, GBG: grain-boundary groove shapes.

Acknowledgements

It is a pleasure to express my gratitude to Prof.Dr. W. Känzig for his guidance, support and constant encouragement.

My special thanks are due to Dr. J. Bilgram for having grown the crystals, for his help during the measurements and for many fruitful discussions.

The collaboration of H.P. Graf, D. Conti, H.R. Haller and P. Wiltzius is greatfully acknowledged.

I further thank Prof.Dr. G.B. Benedek, Dr. R. Hofmann, Dr. E. Serrallach, Dr. M. Zulauf and Dr. H.R. Tschudi for helpful discussions.

I also thank Miss O. Rösli for having typed the manuscript. Finally, I thank my wife and all my colleagues in the solid state laboratory for their support.

Zusammenfassung

Die Dynamik des Gefrierprozesses wird an der Phasengrenze Eis-Wasser mit Rayleighspektroskopie untersucht. Kritisch für das Experiment ist die Reinheit des Wassers und des Eises. Die Reinigung des Materials geschieht durch Zonenschmelzen. Dabei sind etwa 15 Durchgänge notwendig. Um Verunreinigungen durch das Experiment zu vermeiden muss in situ während des Zonenschmelzens gemessen werden. Man beleuchtet die Basalebene des in c-Richtung wachsenden Eis-Einkristalls mit einem Argon-Laser (λ = 488 nm) in streifendem Einfall. Die Streuebene liegt praktisch in der Basalebene. Die Detektion des gestreuten Lichtes geschieht mit einem Photomultiplier.

Die Intensität des Streulichtes als Funktion der Wachstumsgeschwindigkeit zeigt ein Hysteresisverhalten, derart dass eine frisch angeschmolzene Oberfläche keine Lichtstreuung zeigt bis die Wachstumsgeschwindigkeit einen kritischen Wert übersteigt. Dann tritt an der Phasengrenze eine über den Untergrund hinausgehende Streuintensität auf, die proportional zur Wachstumsgeschwindigkeit ist und erst wieder verschwindet, wenn die Oberfläche angeschmolzen wird.

Die Linienbreite des gestreuten Lichtes ist proportional zum Quadrat des Streuvektors und beträgt bei einem Streuwinkel von 90^{o} etwa 2 krad/s. Die Linienbreite ist unabhängig von

der Wachstungsgeschwindigkeit. Gemessen wurde bei Geschwindigkeiten zwischen 0,03 und 2,5 µm/s.

Die Untersuchung der räumlichen Kohärenz des gestreuten Lichtes zeigt, dass die streuende Schicht dünner als 6 µm ist.

Die quantitative Interpretation der Messungen erfolgt mit einem Modell, das den exponentiellen Zerfall von Unebenheiten der Grenzfläche beschreibt. Die Gleichgewichtstemperatur einer gekrümmten Oberfläche weicht von der einer ebenen Oberfläche ab. Dies bewirkt das Schmelzen der Berge und Auffüllen der Täler. Die Uebereinstimmung mit den gemessenen Linienbreiten ist gut.

Author		Ref.	σ_{SL} [mJm^{-2}]	T[°C]	method
Fisher et al.	1949	53	32,8		HN
Jacobi	1955	54	24	0	HN
			15,1	-40	
Skapski et al.	1957	55	44±10	0	CC
Kuhns et al.	1968	56	20		HN
Ketcham and Hobbs	1969	52	33±3	0	DAC
Jones	1970	57	26,1		
Wood and Walton	1970	58	31,93±0,44	0	HN
			24,22±0,02	-36,55	
Coriell et al.	1971	59	25±2	≃0	IP
Jones	1973	60	44±10	0	GBG
Jones	1974	57	46		
Hardy	1977	51	29,1±0,8	0	GBG

Table 1

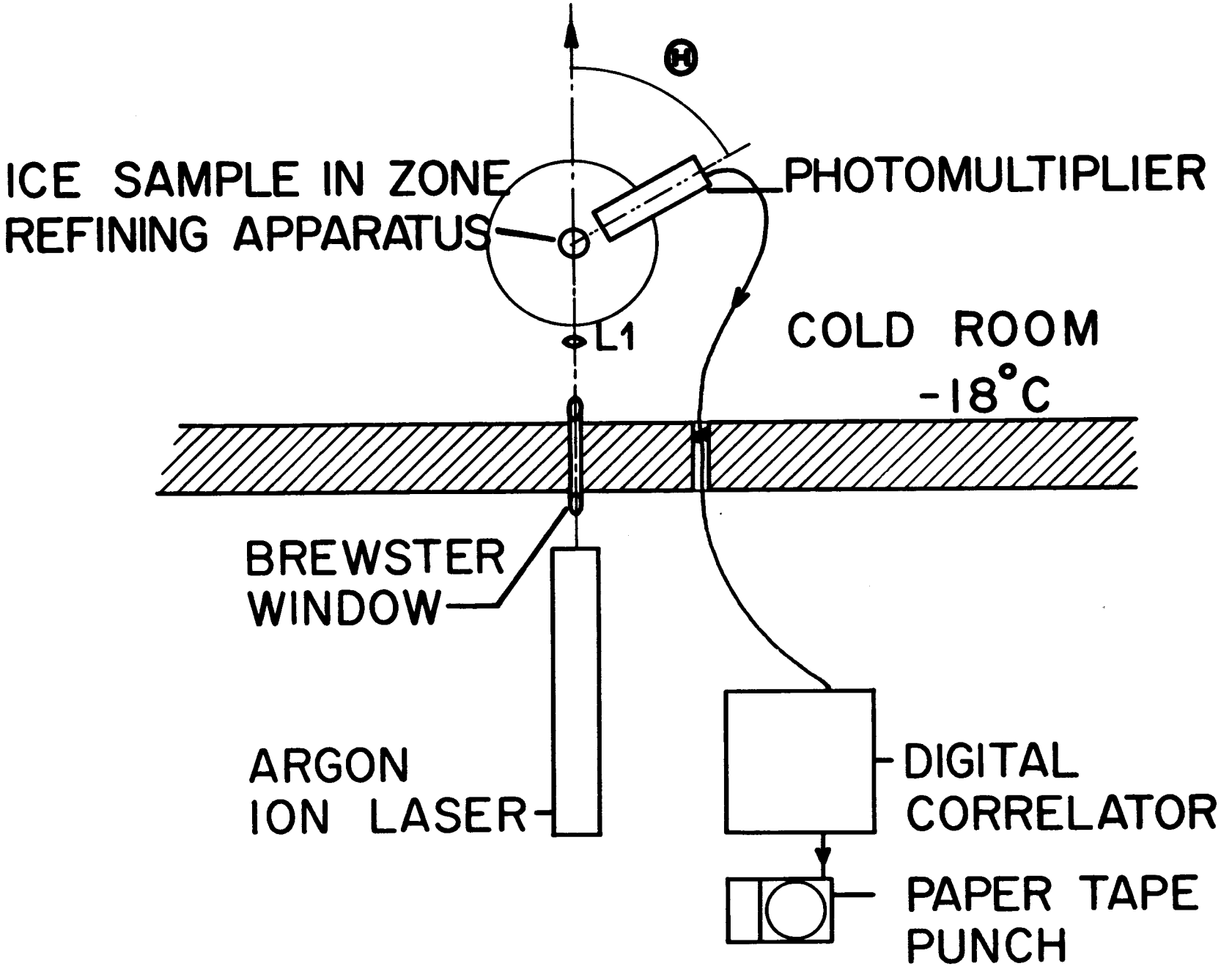
H
ICE SAMPLE IN ZONE
REFINING APPARATUS
PHOTOMULTIPLIER
L1
COLD ROOM
-18°C
BREWSTER
WINDOW
ARGON
ION LASER
DIGITAL
CORRELATOR
PAPER TAPE
PUNCH

fig. 1

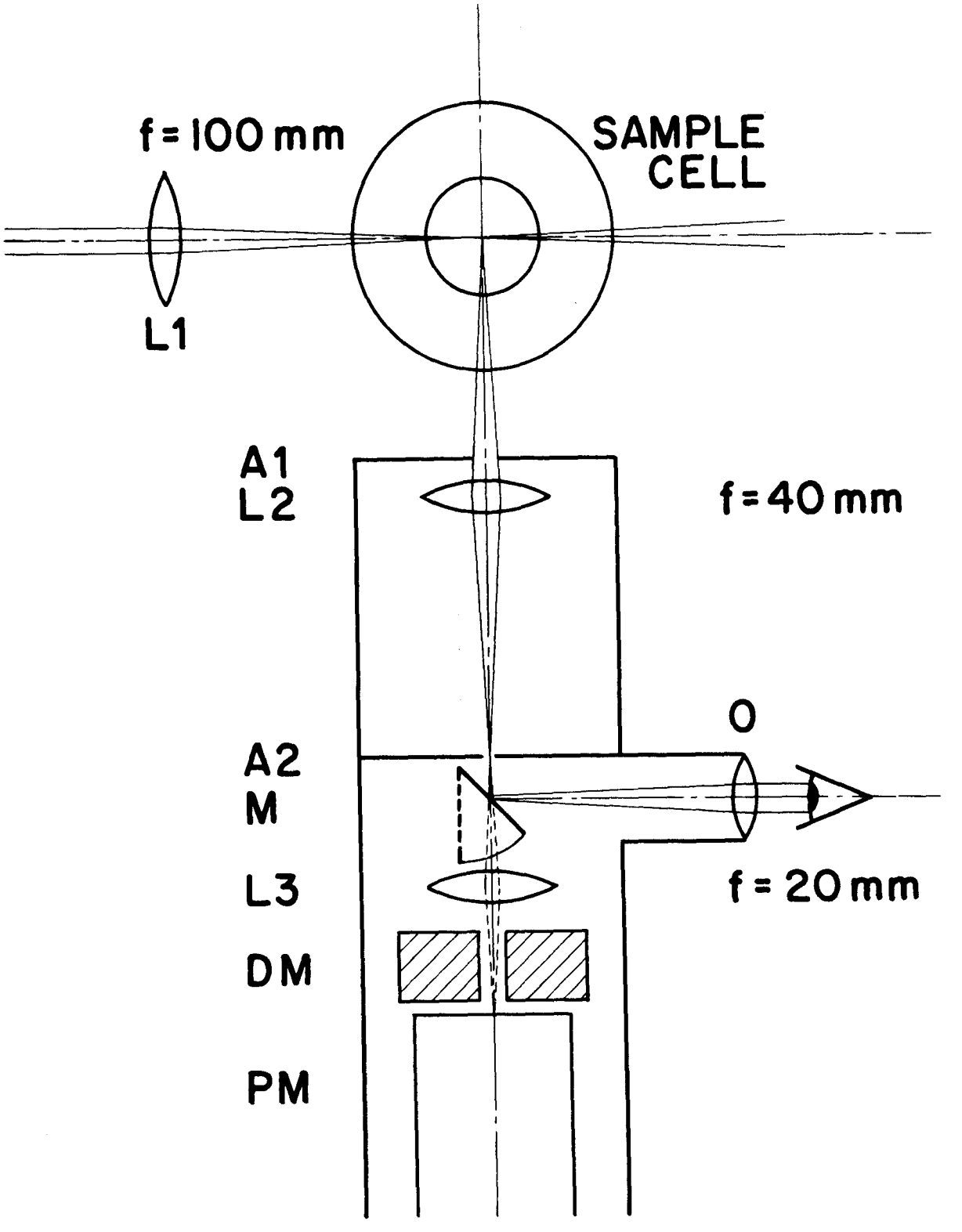

fig. 2

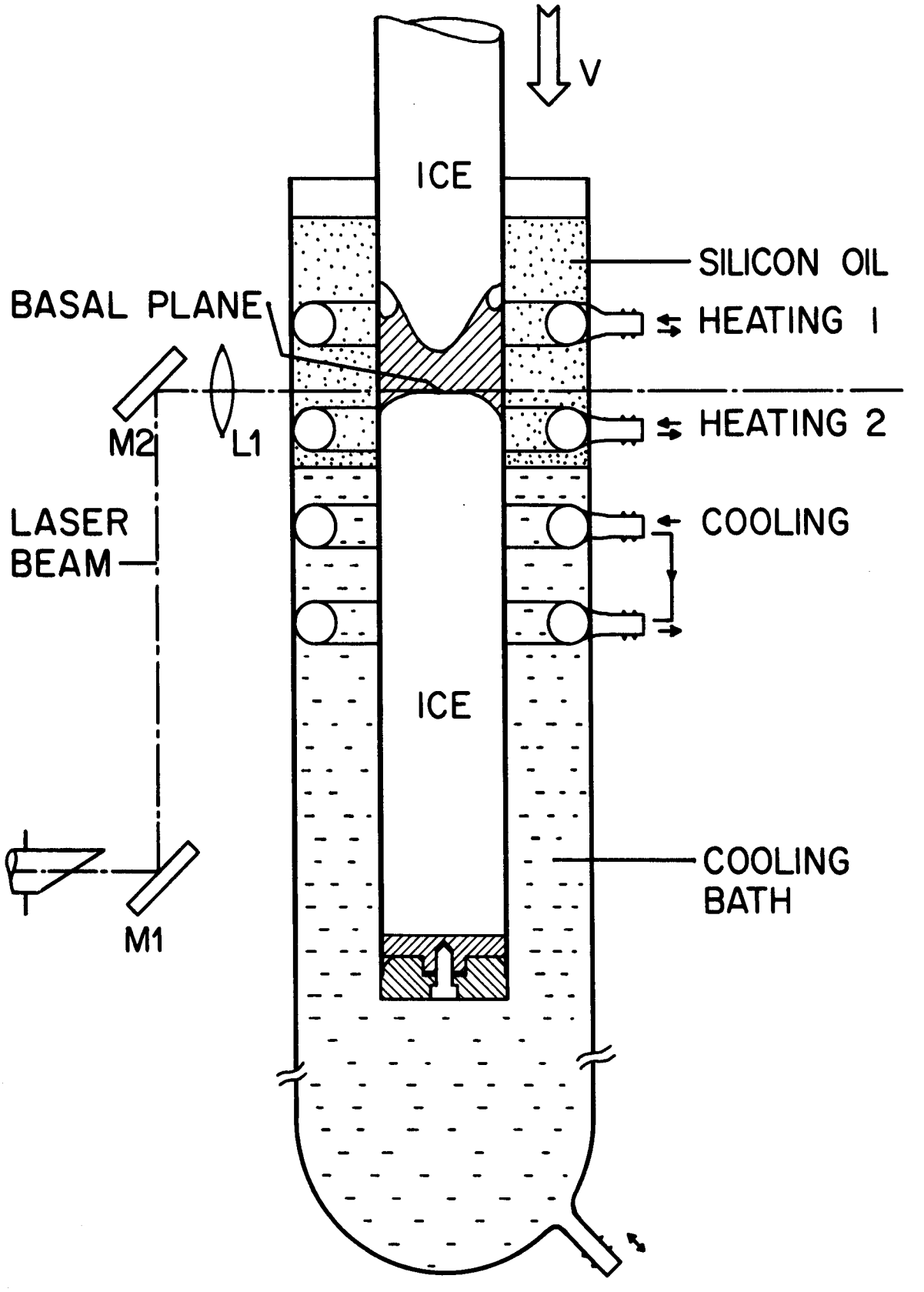
V
ICE
SILICON OIL
BASAL PLANE
HEATING 1
HEATING 2
M2
L1
LASER
BEAM
COOLING
ICE
COOLING
BATH
M1

fig. 3

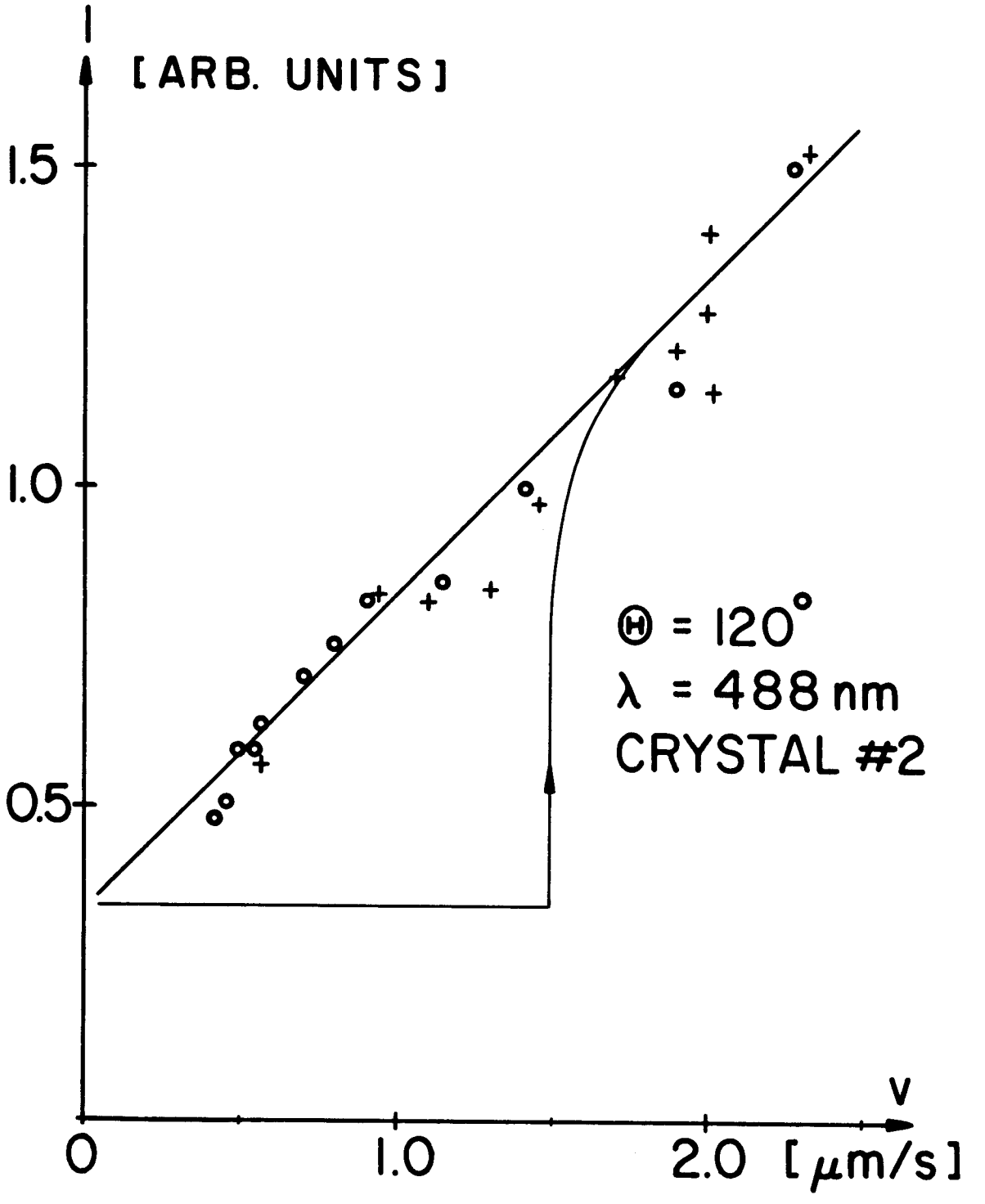

fig. 4

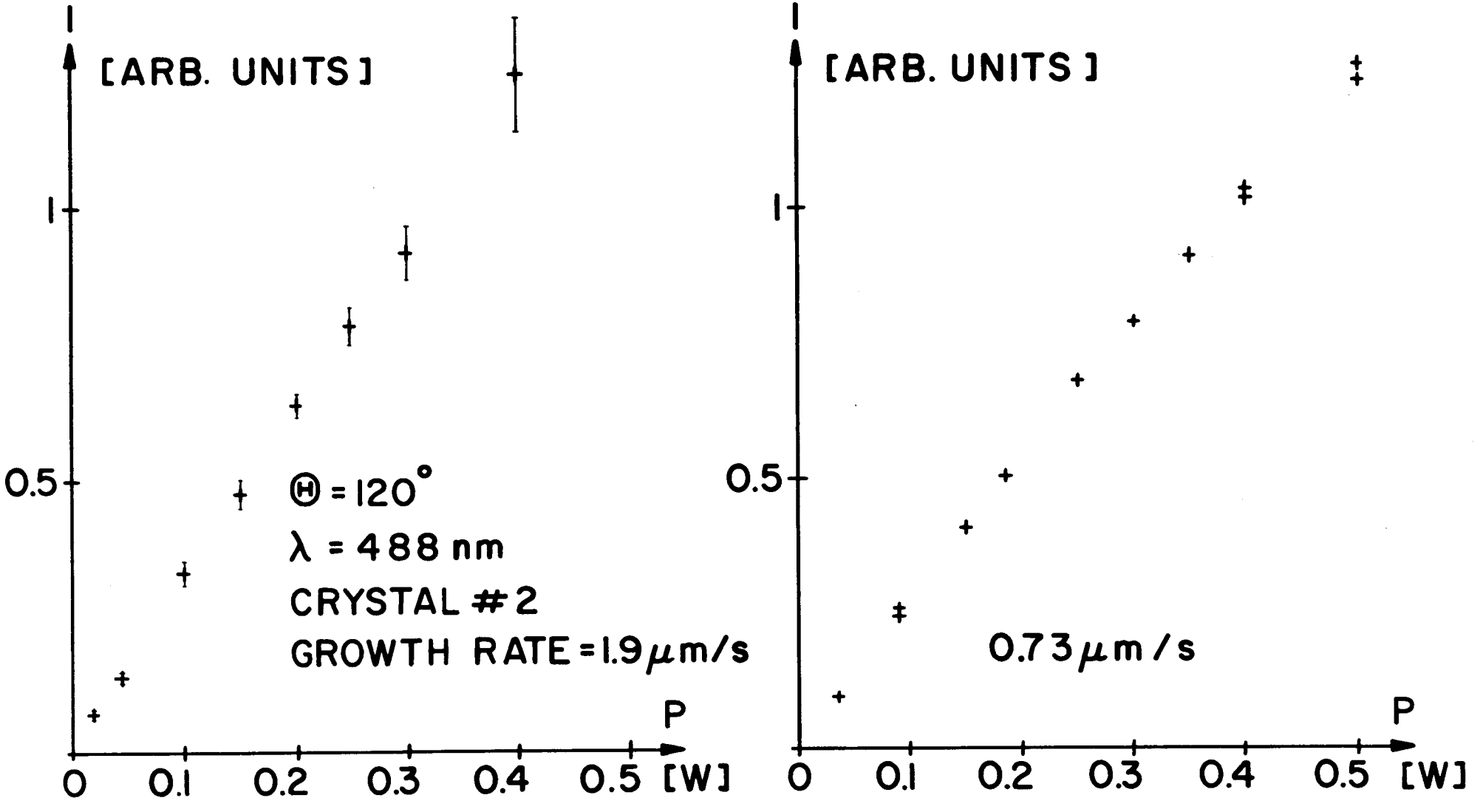
I
[ARB. UNITS]
1
0.5
Θ = 120°
λ = 488 nm
CRYSTAL #2
GROWTH RATE = 1.9 μm/s
P
0
0.1
0.2
0.3
0.4
0.5
[W]
I
[ARB. UNITS]
1
0.5
0.73 μm/s
P
0
0.1
0.2
0.3
0.4
0.5
[W]

fig. 5

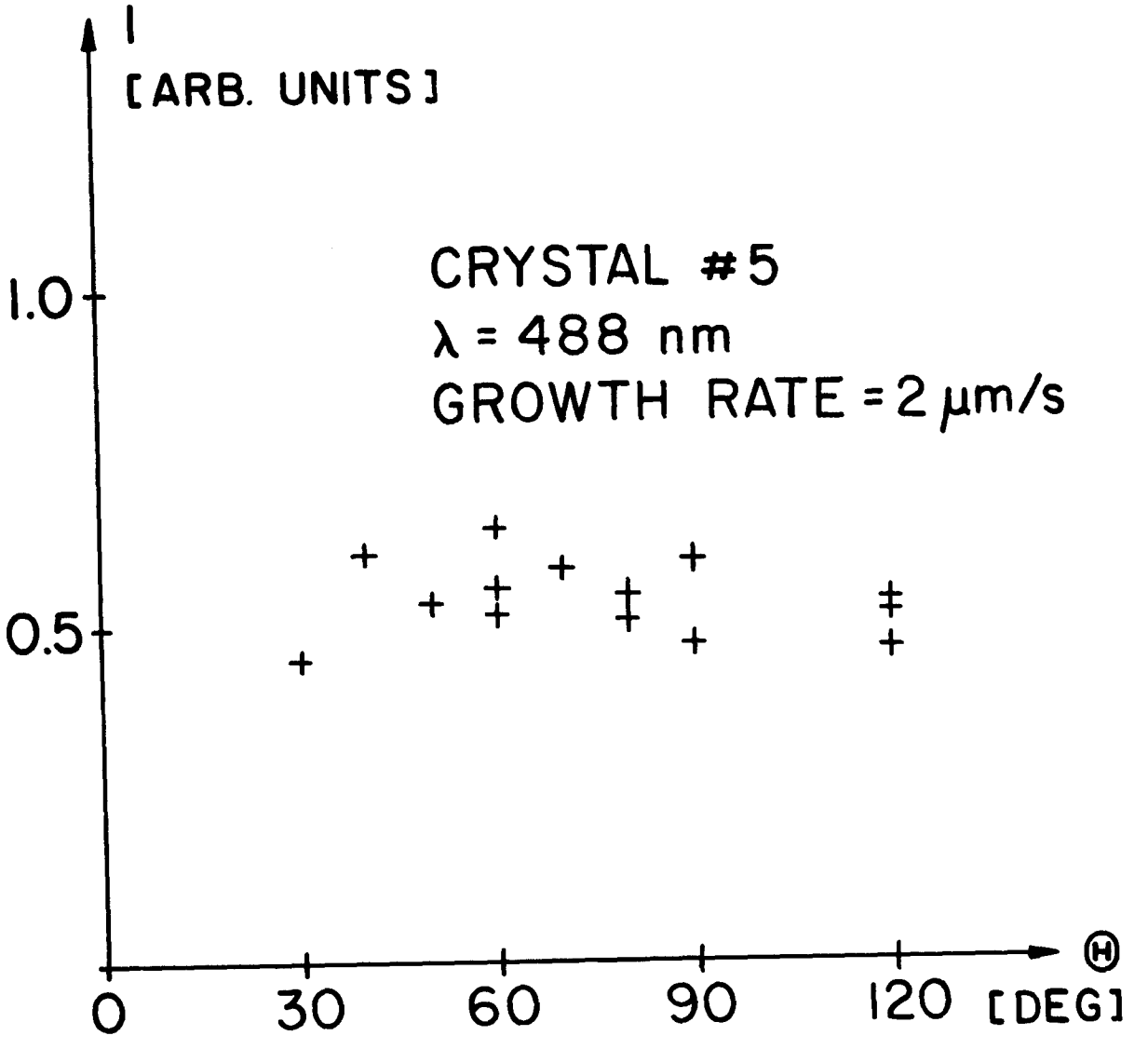
I
[ARB. UNITS]
CRYSTAL #5
λ = 488 nm
GROWTH RATE = 2 μm/s
1.0
0.5
0
30
60
90
120
[DEG]
Θ

fig. 6

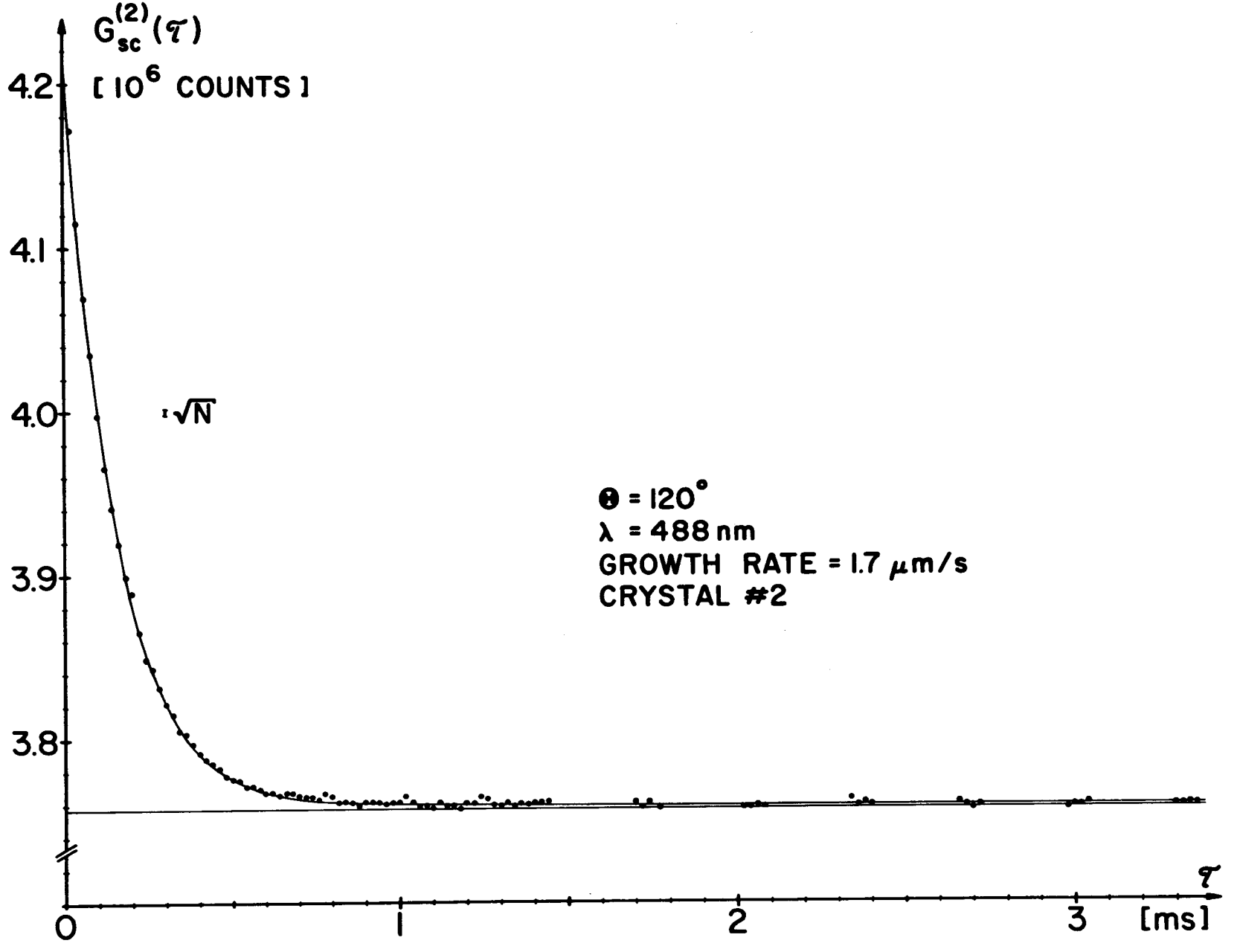
$G^{(2)}_{sc}(\tau)$
[10^6 COUNTS]
4.2
4.1
4.0
3.9
3.8
$\pm\sqrt{N}$
$\theta = 120°$
$\lambda = 488\,nm$
GROWTH RATE = 1.7 $\mu m/s$
CRYSTAL #2
0
1
2
3
[ms]
τ

fig. 7

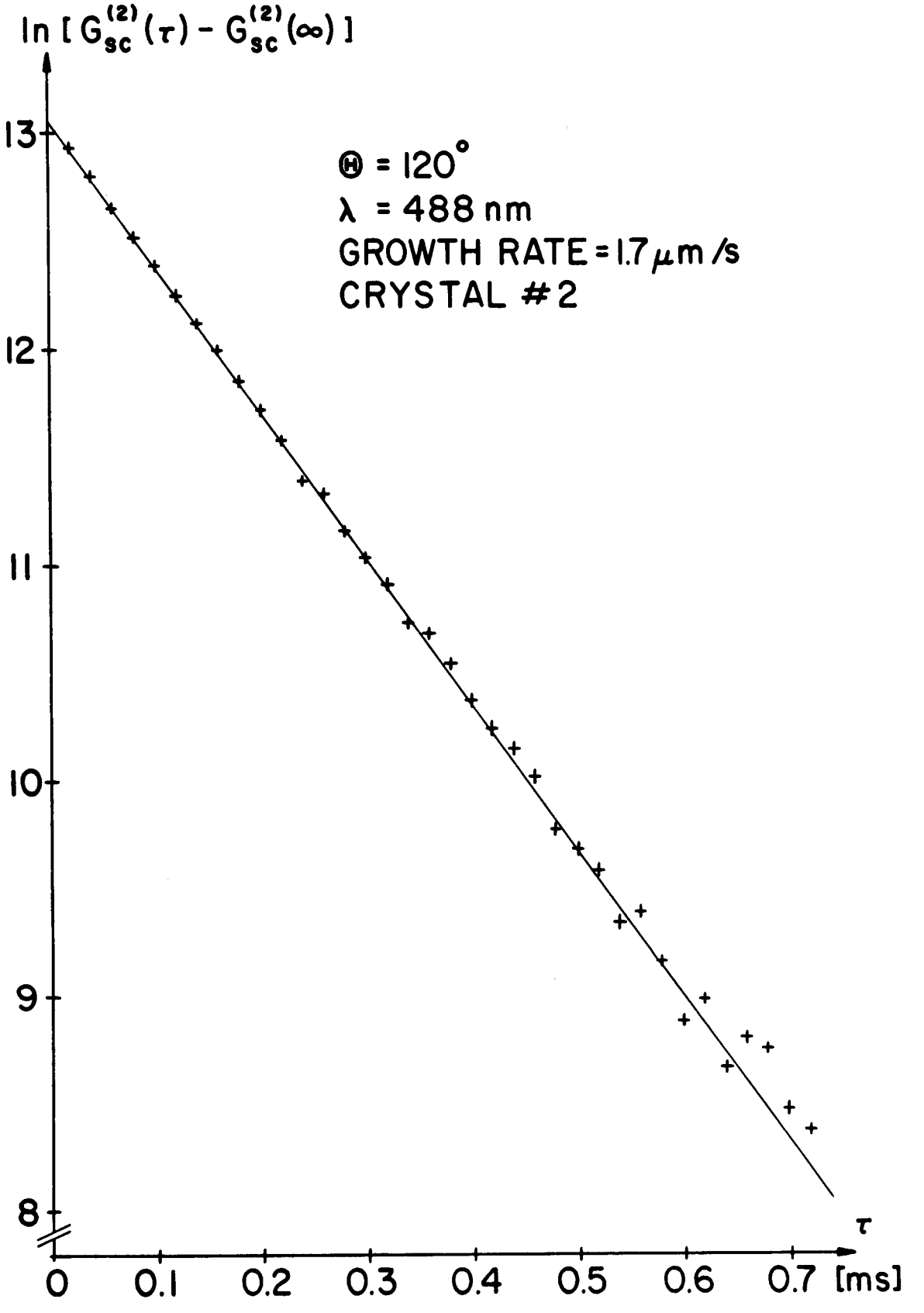
ln [G(2)sc (τ) - G(2)sc (∞)]
Θ = 120°
λ = 488 nm
GROWTH RATE = 1.7 μm/s
CRYSTAL #2
13
12
11
10
9
8
τ
0
0.1
0.2
0.3
0.4
0.5
0.6
0.7
[ms]

fig. 8

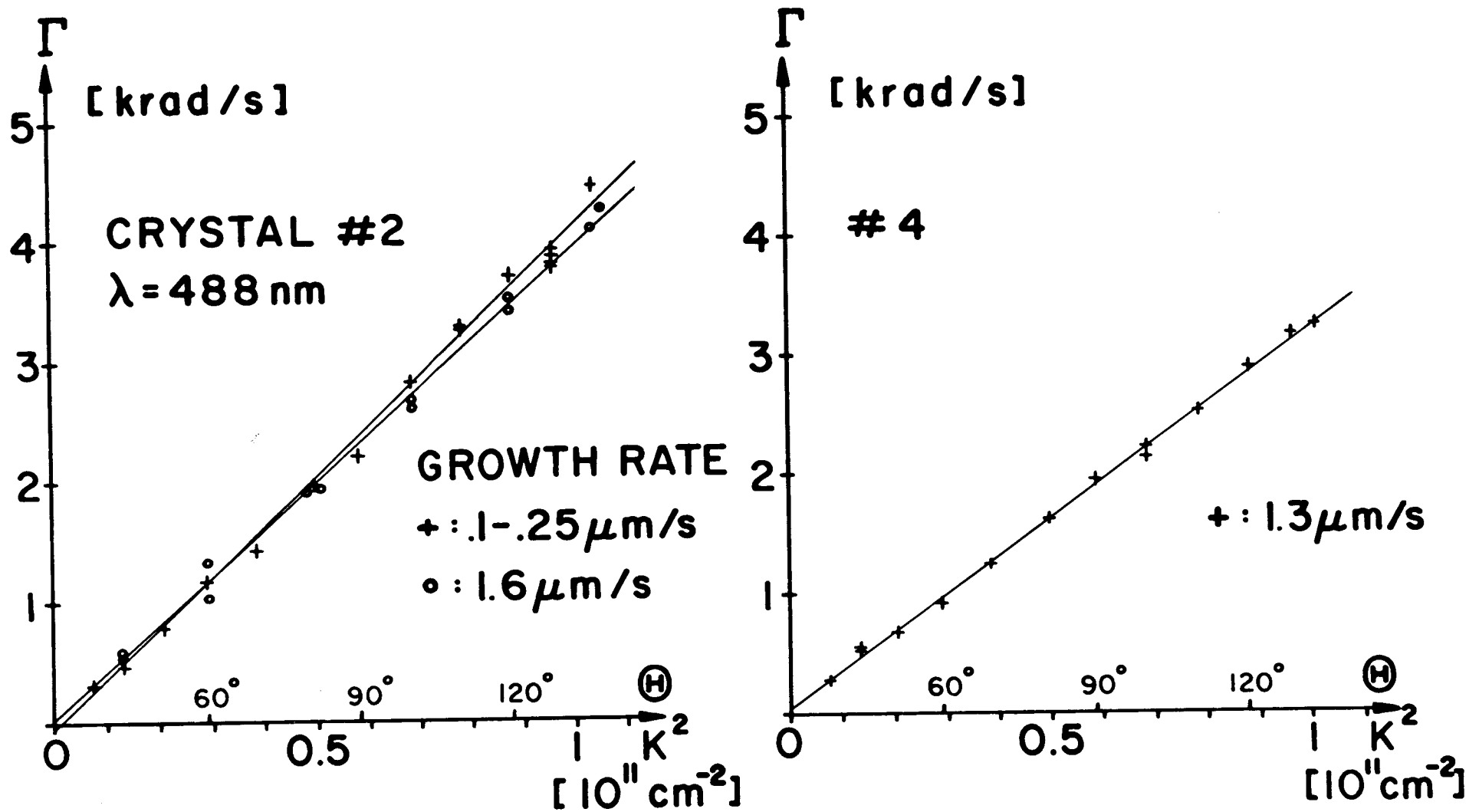
Γ
[krad/s]
5
4
3
2
1
CRYSTAL #2
λ=488 nm
GROWTH RATE
+ : .1-.25 μm/s
o : 1.6 μm/s
60°
90°
120°
Θ
0
0.5
1
K²
[10¹¹ cm⁻²]
Γ
[krad/s]
#4
+ : 1.3 μm/s
60°
90°
120°
Θ
0
0.5
1
K²
[10¹¹cm⁻²]

fig. 9

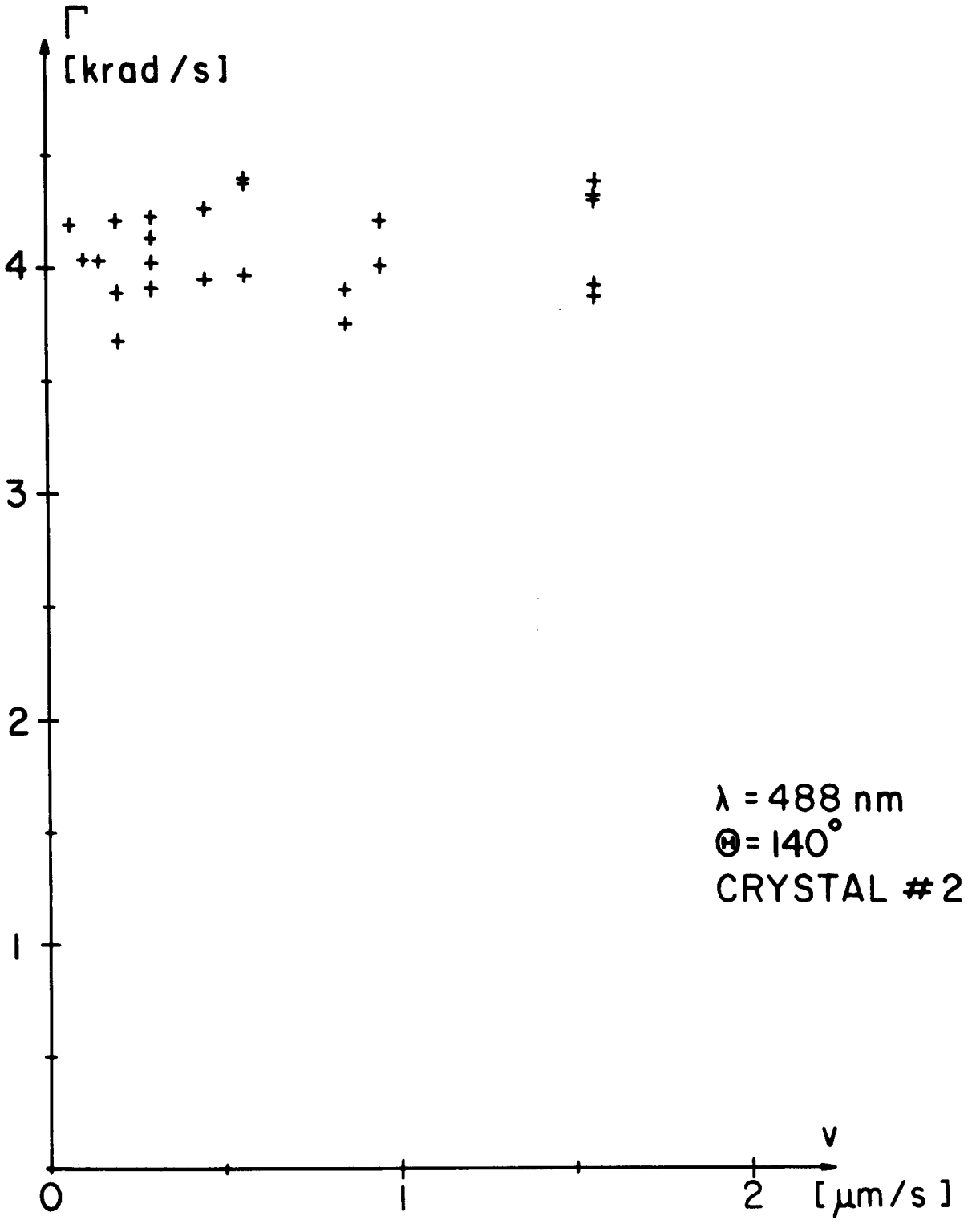

fig. 10

fig. 11

fig. 12

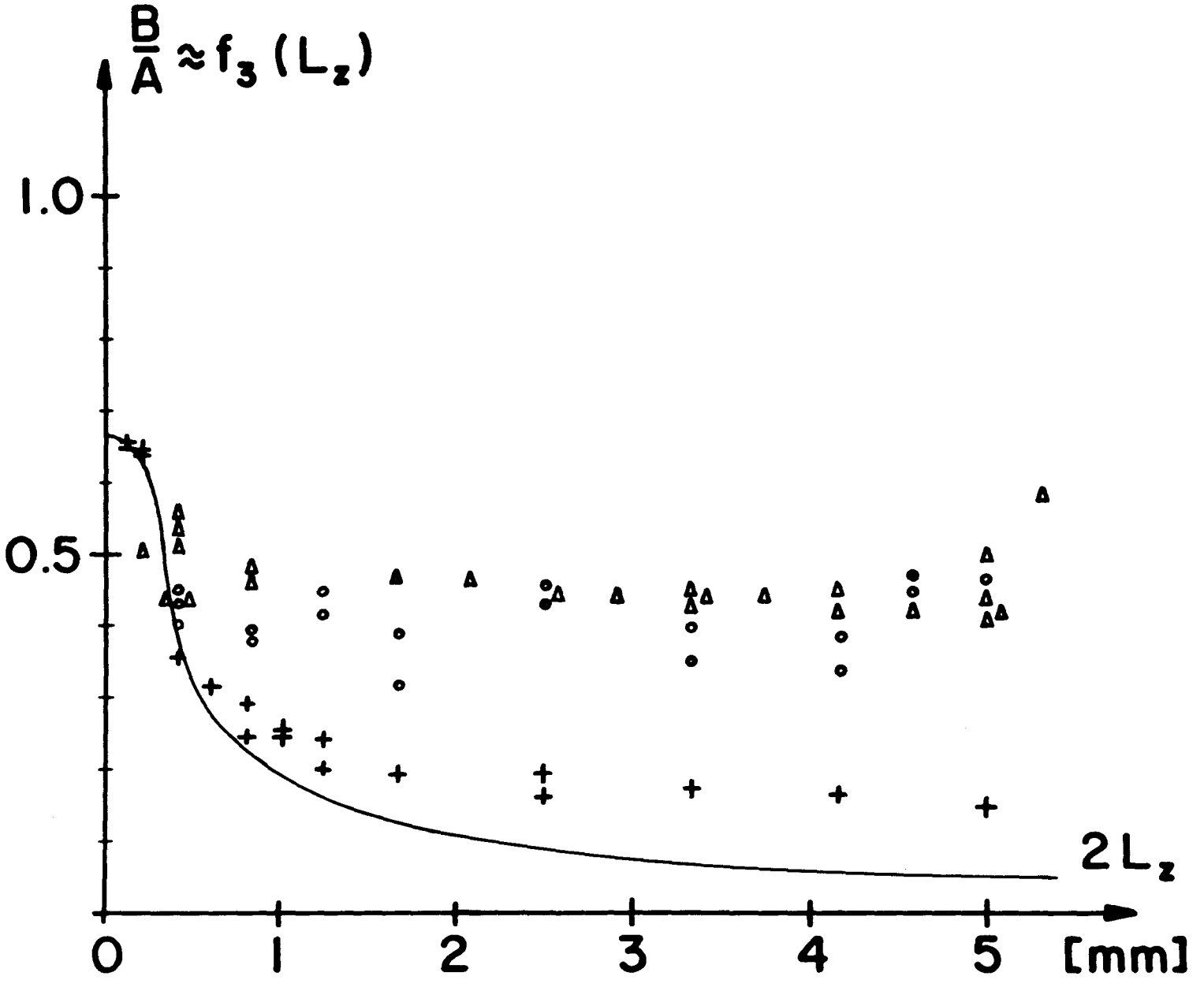

fig. 13

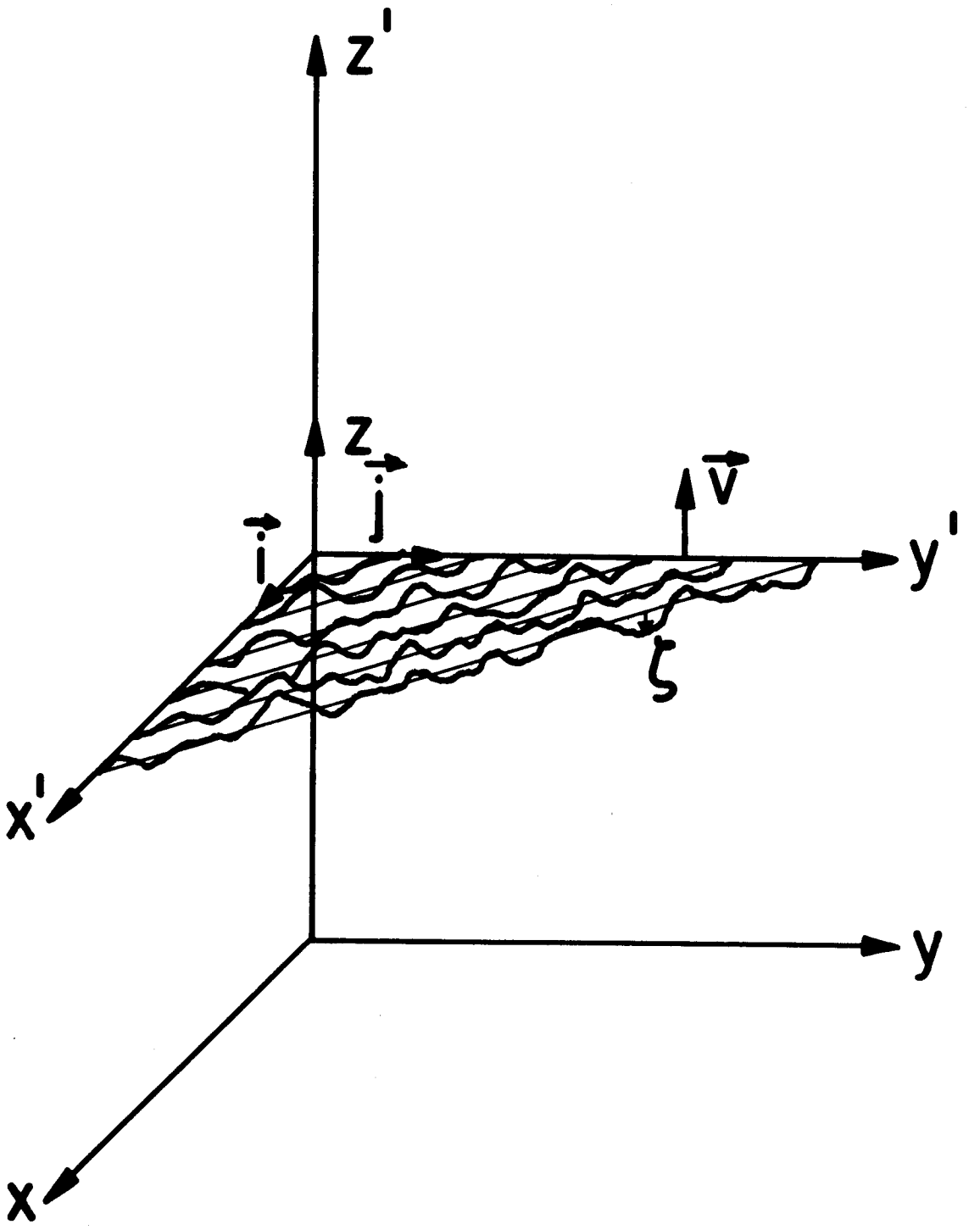

fig. 14

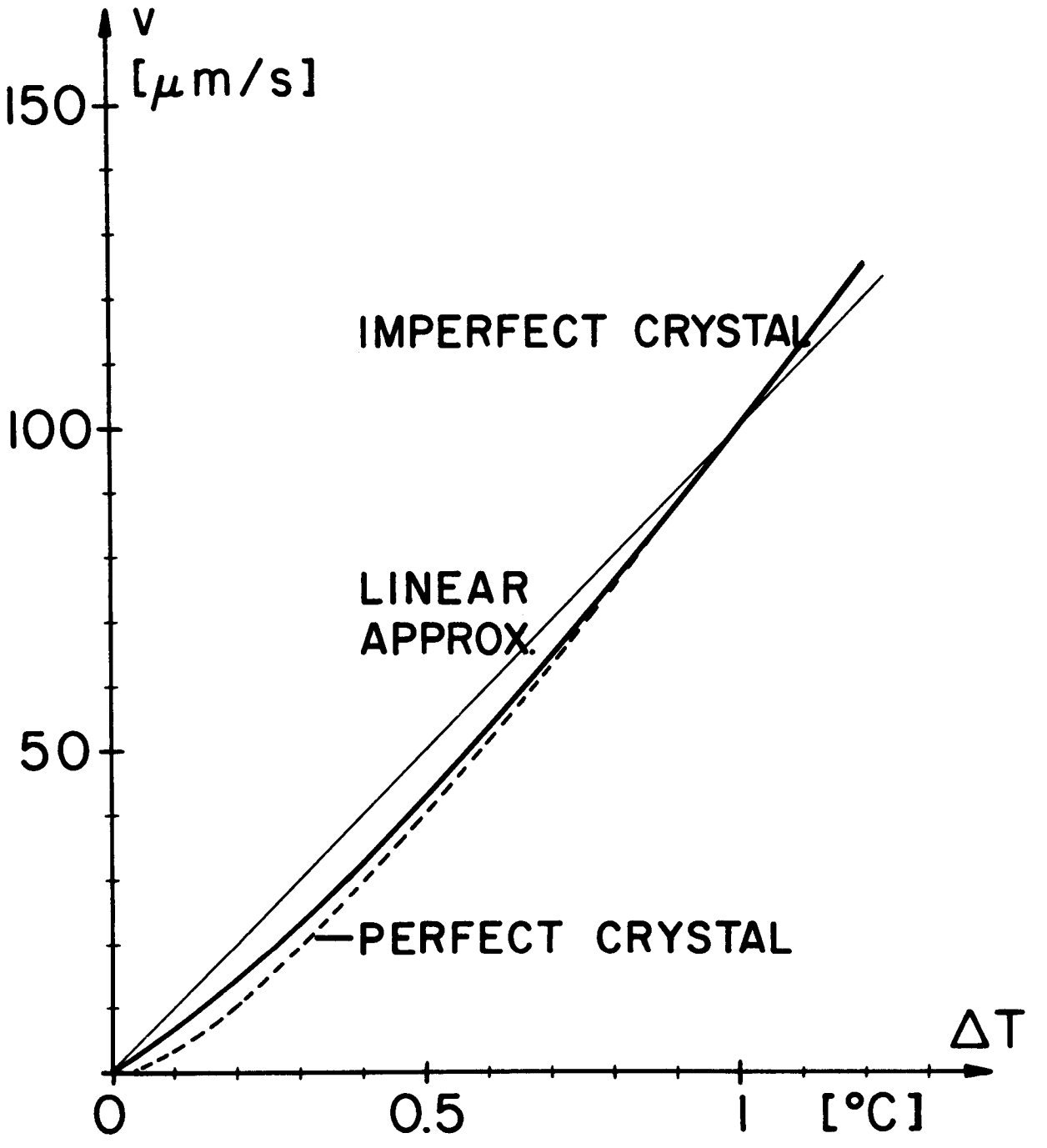
v
[μm/s]
150
100
50
IMPERFECT CRYSTAL
LINEAR
APPROX.
PERFECT CRYSTAL
ΔT
0
0.5
1
[°C]

fig. 15

Biographical notes

Hannes Güttinger was born on December 4, 1946, in Zurich, Switzerland. He attended primary and secondary schools in Zurich. He learned the profession of an architectural draftsman. He then attended a preparatory school (from 1965 to 1968) and passed the Federal Matura exam qualifying him for admission to the Swiss universities. From 1968 to 1973 he attended the Federal Institute of Technology (ETH) in Zürich and received the diploma of Physics. In 1973 he joined the laboratory of solid state physics at the ETH as a candidate for the Ph.D. (1973/74 Prof.Dr. H. Gränicher, 1975 - 1978 Prof.Dr. W. Känzig).